Journal of Solid State Chemistry 183 (2010) 2133–2143

Contents lists available at ScienceDirect

Journal of Solid State Chemistry

journal homepage: www.elsevier.com/locate/jssc

Dependence of the lone pair of bismuth on coordination environment and pressure: An *ab initio* study on $Cu_4Bi_5S_{10}$ and Bi_2S_3

Lars Arnskov Olsen [a,*], Javier López-Solano [b,1], Alberto García [c], Tonči Balić-Žunić [a], Emil Makovicky [a]

[a] Department of Geography and Geology, University of Copenhagen, 1350 Copenhagen, Denmark
[b] Departamento Física de la Materia Condensada, Universidad del País Vasco, 48080 Bilbao, Spain
[c] Institut de Ciencia de Materials de Barcelona (ICMAB-CSIC), Campus UAB, 08193 Bellaterra, Spain

ARTICLE INFO

Article history:
Received 27 January 2010
Received in revised form
27 June 2010
Accepted 3 July 2010
Available online 6 August 2010

Keywords:
DFT
Sulfosalt
Lone electron pair
Electronic structure
High pressure

ABSTRACT

DFT calculations have been carried out for $Cu_4Bi_5S_{10}$ and Bi_2S_3 to provide an analysis of the relation between electronic structure, lone electron pairs and the local geometry. The effect of pressure is considered in Bi_2S_3 and the results are compared to published experimental data. Bi^{3+} in $Cu_4Bi_5S_{10}$ is found at both symmetrically and asymmetrically coordinated sites, whereas the coordination environments of Bi in Bi_2S_3 are asymmetric at room conditions and get more regular with increasing pressure. The charge density maps of the asymmetric sites show the lone pairs as lobes of non-shared charge. These lobes are related to an effective Bi *s*–Bi *p* hybridization resulting from coupling to S *p* orbitals, supporting the modern view of the origin of the stereochemically active lone pair. No effective Bi *s*–*p* hybridization is seen for the symmetric site in $Cu_4Bi_5S_{10}$, whereas Bi *s*–*p* hybridization coexists with a much reduced lone pair in Bi_2S_3 at high pressure.

1. Introduction

The coordination environment of a cation with a single filled *s*-orbital in the last valence shell (like Sn^{2+}, Sb^{3+}, Tl^{+}, Pb^{2+} and Bi^{3+}) is in most crystal structures highly asymmetric. Traditionally the two electrons in the *s*-orbital have been regarded as a lone pair and the distortion of the coordination environment has been explained as accommodating the spatial requirements of this inert pair, which points away from the shortest bonds in the coordination polyhedron.

As the distortion of the coordination environment cannot be explained as an effect coming from the symmetric *s*-orbital, Orgel [1] put forward the idea that the hybridization of cation *s* and *p* orbitals is at the root of the lone pair behavior. This hybridization was meant to be a result of the net crystal field at the cation site, which is determined by the coordination environment, and in particular by the nature of the surrounding anions. For example, the crystal structure of PbO at room conditions is a tetragonal distortion of the cubic rocksalt structure with a stereochemically active lone pair, whereas PbS remains in the undistorted rocksalt structure without any geometrical effect of a lone pair.

New knowledge about the nature of lone pairs emerged from a density functional theory (DFT) study on PbO [2]. The Pb 6*s* electrons were found to take part in bonding with the O 2*p*-electrons and could therefore not be considered as an inert pair. From further DFT studies on PbO, PbS and Sn*X* (*X*=O, S, Se, Te) a more complete lone pair model took form [3–6]. The *s*-orbital of the valence shell of the cation mixes with the *p*-orbitals of the anion creating filled anti-bonding states near the Fermi level. Stabilization of these unfavorable states is possible through a secondary mixing with the *p*-orbitals of the cation. Such mixing is hindered in the highly symmetrical rocksalt-type structure of PbS, where only the primary interactions Pb 6*s*–S 3*p* and Pb 6*p*–S 3*p* are present and separated in energy, but is allowed in the structure of PbO which has a lower symmetry. Fig. 1 shows a schematic orbital diagram which presents the basic ideas of this model.

In this view, the distortion of the coordination environment is caused by the combination of cation *s*, cation *p* and anion *p* orbitals. An asymmetric distribution of charge around Pb is observed in charge density maps from DFT calculations on PbO [5]. Part of the charge is concentrated on the side opposite to the shortest bonds in the coordination polyhedron. A strong localization of this charge, as implied by the term "lone pair", is confirmed by employment of the electron localization function (ELF) [8]. A number of studies on lone pair compounds such as the ternary oxides, $SnWO_4$, $PbWO_4$ and $BiVO_4$ [9] and thallium halides [10] have now reached conclusions in agreement with the model described above.

In this paper we provide a supporting but complementary view for this model based on detailed DFT analyses of the electronic structures of two systems. First, we study $Cu_4Bi_5S_{10}$, a compound that allows us to study Bi^{3+} in both a symmetric and

* Corresponding author.
E-mail address: lao@geo.ku.dk (L.A. Olsen).
[1] Present address: MALTA Consolider Team—Departamento Física Fundamental II, Universidad de la Laguna, 38205 La Laguna, Spain.

0022-4596/$ - see front matter © 2010 Elsevier Inc. All rights reserved.
doi:10.1016/j.jssc.2010.07.022

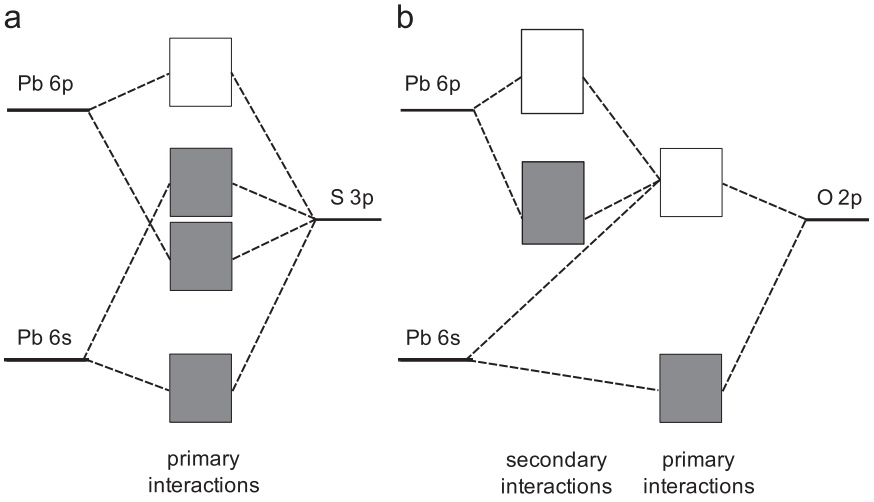

Fig. 1. Schematic orbital diagram for PbS (a) in rocksalt-type structure and PbO (b) with tetragonal symmetry. Shaded blocks represent occupied states. Modified from Yang and Dolg [7].

asymmetric coordination environment in a single crystal structure, with a single type of anion. The former coordination is unusual for Bi in sulfides.

The crystal chemical behavior of the lone pair elements Pb^{2+} and Bi^{3+} has been studied in detail in a series of high pressure experiments with single crystal X-ray diffraction on sulfosalts and sulfides of metalloids [11–14]. The distortion of a coordination polyhedron can be quantified by the cation eccentricity which is defined as the displacement of the cation from the centroid (ideal center) of the coordination polyhedron divided by the fitted-sphere radius [15]. The cation eccentricity is taken as a measure of the stereochemical activity of the lone pair. The general behavior of the Pb and Bi polyhedra is a decreasing cation eccentricity, i.e. less distortion, at increasing pressure as long as no phase transition is observed. This leads to the crystal chemical interpretation of a less stereochemically active lone pair at higher pressure.

The second part of the paper presents an analysis of the effect of pressure on the lone pair and the related electronic configuration of bismuthinite (Bi_2S_3). Bismuthinite is a simple representative of a compound for which experiments have shown that the distorted coordination environments around Bi^{3+} get more regular with increasing pressure [12].

Our work combines the knowledge that can be obtained from DFT calculations with the geometrical and crystal chemical approaches, providing an analysis of the electronic structure and its relation to the geometry of the coordination environment.

2. Computational methods

We employ the SIESTA DFT code [16], which is ideally suited to analyze bonding effects due to its use of a basis set of finite-range atomic-like orbitals. It also offers other powerful tools for electronic-structure analysis, among them energy-resolved pseudo-charge density maps, the projected density of states (PDOS), and the crystal orbital Hamilton population (COHP), the latter giving the bonding or anti-bonding character of orbital interactions [17]. All the calculations use norm-conserving pseudopotentials and the PBE exchange-correlation functional [18].

Pseudopotentials were generated with the following valence configurations: $6s^2\ 6p^3\ 6d^0\ 5f^0$ for Bi, $3s^2\ 3p^4\ 3d^0\ 4f^0$ for S and $4s^1\ 4p^0\ 3d^{10}\ 4f^0$ for Cu. Cutoff radii were taken close to the outer maximum of the atomic wavefunctions. With shorter radii, no major differences were found in the density charge maps for the areas close to the atomic cores, where the effects of lone pairs can be observed. This remains true even when high pressure is applied to Bi_2S_3.

The pseudo-atomic-orbital (PAO) basis sets used in the calculations included two orbitals for each occupied electronic state, and one for each unoccupied state. The radii of the basis functions were optimized following the method described in Ref. [19]. Convergence tests on the energy were performed to obtain the mesh cutoff parameter (which controls the fineness of the real space grid used to perform real space integrations) and number of k points (used to approximate reciprocal space integrations). For $Cu_4Bi_5S_{10}$, a mesh cutoff of 7500 eV and 10 *k* points were used, whereas the corresponding values for Bi_2S_3 are 10000 eV and 36 *k* points. Using these parameters and starting from experimental data we performed a full optimization of the atomic positions and cell parameters of each structure considered, reaching atomic forces lower than 0.005 eV/Å, and differences in the stress tensor components of less than 0.1 GPa.

3. $Cu_4Bi_5S_{10}$

The crystal structure of synthetic[2] $Cu_4Bi_5S_{10}$ [20] is monoclinic *C2/m* with two distinct positions for Cu and three distinct positions for Bi (Fig. 2). The two Cu-sites are coordinated by tetrahedra of sulfurs. The point symmetry of the Bi1 site is *2/m* but it is coordinated by an almost perfect octahedron, with four S-atoms (S1) forming the equatorial plane perpendicular to the mirror plane and two S-atoms (S2) in the polar trans-position. The high symmetry of the coordination environment is unusual for a Bi atom in sulfides. Bi2 and Bi3 are coordinated by distorted mono-capped trigonal prisms and represent the more usual asymmetric coordination environment of Bi. Both sites have three short Bi–S distances and four Bi–S distances which are markedly longer (Table 1). The former can be considered as indicating important bonding interactions, whereas the lone pair is oriented towards the latter. The cation eccentricities of Bi2 and Bi3 are 0.175 and 0.206 (values from *ab initio* calculations), respectively.

[2] The mineral kupčíkite ($Cu_{3.6}Fe_{0.4}Bi_5S_{10}$), a natural iron-containing equivalent to the synthetic $Cu_4Bi_5S_{10}$ has also been described [21]. The crystal structure of kupčíkite is almost identical to $Cu_4Bi_5S_{10}$ with minor variations in lattice parameters and interatomic distances.

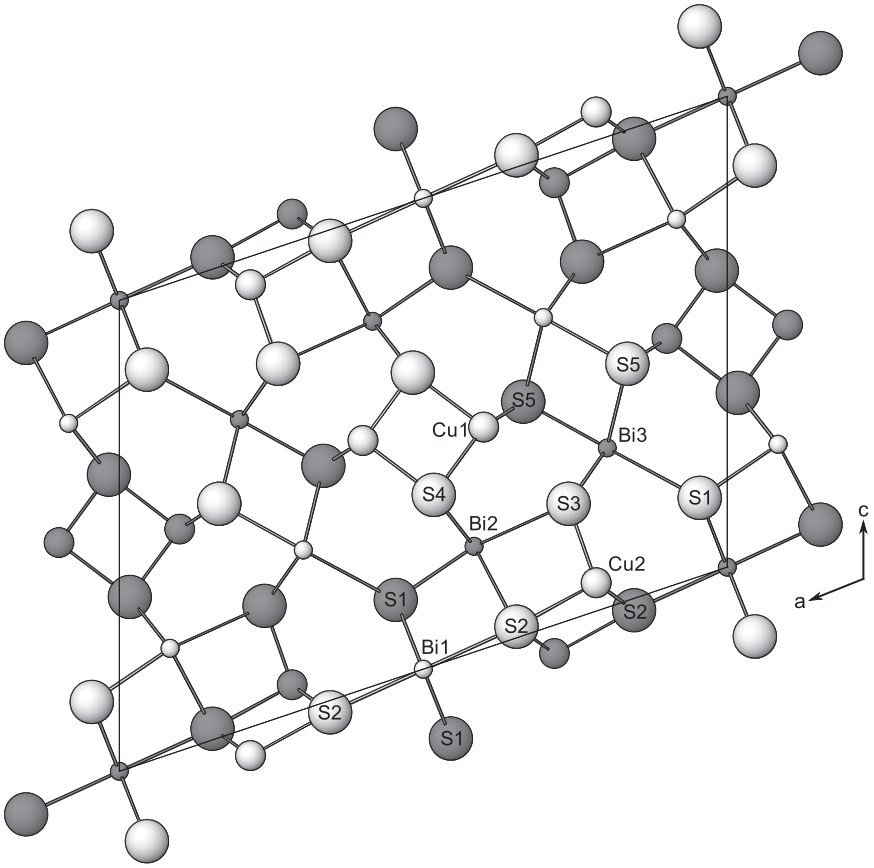

Fig. 2. Crystal structure of $Cu_4Bi_5S_{10}$. Dark circles represent atoms on the $y=0$ mirror plane, white circles represent atoms on the $y=0.5$ mirror plane.

Table 1
Comparison of bond lengths (Å) in the *ab initio* and synthetic [20] $Cu_4Bi_5S_{10}$ crystal structures.

Bond	*Ab initio*	Synthetic
Bi1–S1 (× 4)	2.84	2.85
Bi1–S2 (× 2)	2.84	2.82
Bi2–S1	2.64	2.62
Bi2–S4 (× 2)	2.70	2.67
Bi2–S2 (× 2)	3.14	3.13
Bi2–S3 (× 2)	3.40	3.42
Bi3–S5	2.66	2.63
Bi3–S3 (× 2)	2.72	2.74
Bi3–S5 (× 2)	3.10	3.04
Bi3–S1 (× 2)	3.56	3.51

Starting from the experimental data a full optimization of the lattice parameters and atomic positions was performed. This optimized structure has been used in all the remaining calculations. The equilibrium (zero pressure) volume obtained in the calculations is 428.9 $Å^3$ per formula unit, in fair agreement with the experimental value of 421.2 $Å^3$ [20], with the usual overestimation caused by the GGA approximation. Table 1 compares the Bi–S interatomic distances for the *ab initio* and experimental structures. Cu–S bond lengths show a similar agreement.

3.1. Electronic structure of $Cu_4Bi_5S_{10}$

The PDOS and COHP have been calculated in order to examine the electronic structure of $Cu_4Bi_5S_{10}$ and get a quantitative measure of the Bi–S interactions. The main S *s* states lie between −18 and −16 eV. From preliminary tests these S states are found to have a small effect on the higher part of the valence band and on the electronic features relevant to this work. Also note that in most of the preceding studies on lone pairs the *s*-electrons in the valence shell of the anion were left out from the treatment of chemical bonding, as they are considered to be semi-core electrons and hence chemically inactive. Therefore we only take the S 3*p* orbitals into further consideration. In the same way, as the aim of this study is an investigation of Bi–S interactions, we do not go into details of the Cu–S interactions. To enhance the readability the *n* quantum number is taken as implicit in the subsequent text since only the highest levels, 6 for Bi and 3 for S, are considered.

The PDOS decomposed by *l*-quantum number is shown in Fig. 3. For simplicity only one of the asymmetric Bi sites (Bi2) is shown along with the symmetric Bi site (Bi1) and two S sites (S1 and S2). The calculations for Bi3 are presented in the Supplementary Material. The properties of the two asymmetric Bi sites are almost identical and the properties of other S atoms are intermediate between S1 and S2. The energy range from −15 eV to the Fermi level around −4 eV presents the valence band, whereas the lowest part of the conduction band lies from −3 to 0 eV.

The PDOS is distributed in three regions separated by two band gaps. Region I between −15 and −13 eV is split off from the upper part of the valence band and consists mainly of Bi *s* states with small contributions of S *p* states. Region II (IIa and IIb) from −10 to −4 eV has mainly S *p* and Bi *p* character, but also some Bi *s* states are present. Region III features mainly Bi *p* states, along with some contributions of S *p* states.

Region II has been divided in two subregions in some of the previous studies on lone pairs [5,10]. Such subdivision is most relevant for the Bi1 position where the Bi *s* states are concentrated

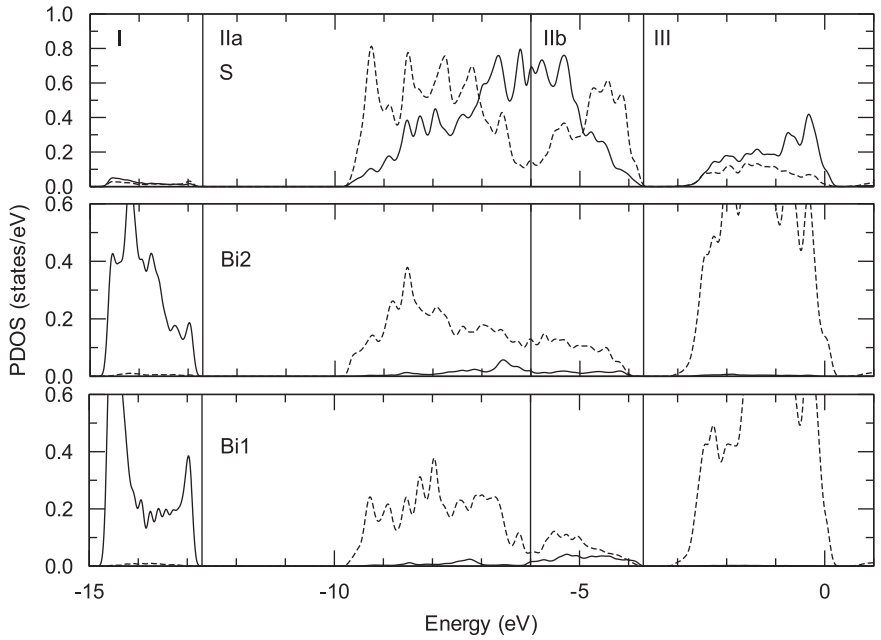

Fig. 3. PDOS plot for $Cu_4Bi_5S_{10}$. Top panel: solid and dashed lines are S1 *p* and S2 *p*, respectively. Middle and bottom panels: solid and dashed lines are Bi *s* and Bi *p*, respectively.

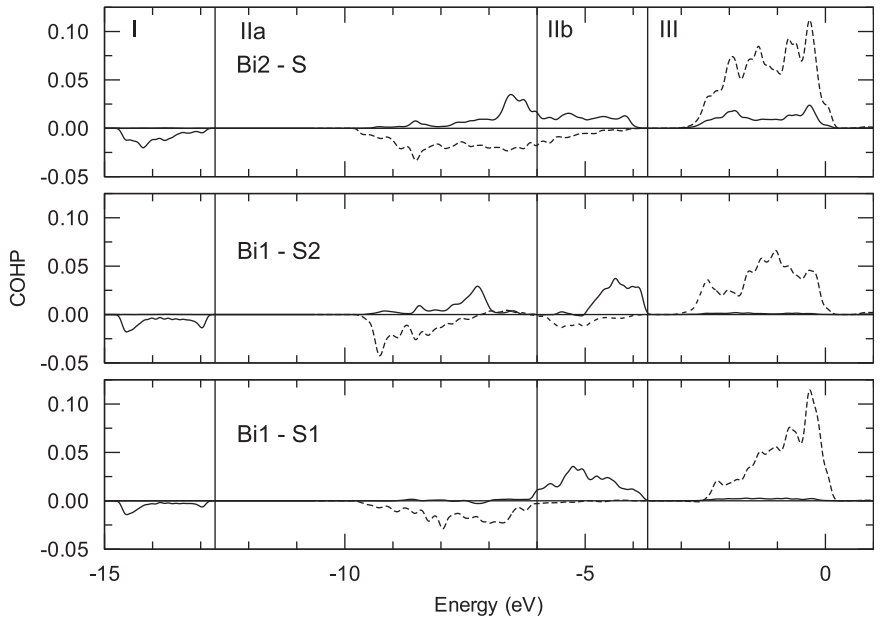

Fig. 4. COHP per bond for the Bi2–S (only S1 and S4 are taken into account), Bi1–S2 and Bi1–S1 interactions in $Cu_4Bi_5S_{10}$. Solid lines are used for Bi *s*–S *p* interactions, dashed for Bi *p*–S *p*. A negative COHP value means a bonding interaction.

at the top of the band (region IIb), whereas Bi *p* states are mainly concentrated in the lower part of the band (region IIa). For the Bi2 site a broader distribution of Bi *s* and Bi *p* states, with no separations, is seen in region II.

The Bi–S interactions and their bonding/anti-bonding character can be studied in Fig. 4 where the COHP per bond is shown. The COHP for Bi1–S was found to have a strong dependence on the direction and is therefore decomposed into Bi1–S2 interactions and Bi1–S1 interactions. The COHP for Bi2–S is shown as an average over the three shortest bonds. Quantitative details of each interaction are given in Table 2 which shows the integration of the COHP (ICOHP).

The Bi *s* and S *p* states described in region I of the PDOS produce a bonding Bi *s*–S *p* interaction in region I of the COHP. The corresponding anti-bonding interaction is distributed in regions II and III for Bi2–S, in region II for Bi1–S2 and exclusively in region IIb for Bi1–S1. Bi *p*–S *p* bonding is observed in region II for Bi2–S and Bi1–S2, and only in region IIa for Bi1–S1. Bi *p*–S *p* anti-bonding is limited to the conduction band in region III.

The ICOHP in Table 2 confirms that the three short bonds (one Bi2–S1 and two Bi2–S4) represent the main interactions in the Bi2 polyhedron. The Bi2–S2 bond of intermediate length has markedly weaker interactions and the interactions between Bi2 and S3 are further reduced.

The features of the COHP for Bi1–S1 can easily be understood by looking at the orbital diagram for a structure with high symmetry (Fig. 1a). Only the Bi *s*–S *p* and Bi *p*–S *p* interactions are needed to explain the COHP in the four regions, and the boundary between the IIa and IIb regions can be seen to correspond roughly to the position of the S *p* level. The COHP for the Bi2–S and Bi1–S2 interactions are more complex, with a broader distribution and in particular a significant overlap of Bi *s*–S *p* and Bi *p*–S *p* weight in region II. From a fundamental point of view, the overlap would seem to reflect the participation of all three types of orbitals (Bi *s*, Bi *p* and S *p*) in the same wavefunctions, a configuration which is usually associated with the lone pair. In particular, Bi *s* and Bi *p* would be mixed in the wavefunctions as a kind of local cation hybrid. This view could be understood in terms of the so-called "secondary interactions" in the orbital diagram for low symmetry structures (Fig. 1b).

However, in some cases the analysis of the overlap of the COHP (or PDOS) curves may not be enough to determine if two orbitals are hybridized. The overlap might simply be the result of the existence of separate bands (i.e., separate wavefunctions) with the appropriate character in the same energy range. A proper quantification of the hybridization of two orbitals μ and ν in the same wavefunction can be obtained (in a convenient energy(ε)-resolved form) as

$$Hyb_{\mu\nu}(\varepsilon) = \sum_i |C_{\mu i} C_{\nu i}| \, \delta(\varepsilon - \varepsilon_i) \quad (1)$$

Eq. (1) is basically the COHP expression without the Hamiltonian weight, so that only the wavefunction coefficients $C_{\mu i}$ and $C_{\nu i}$ appear, with i as the wavefunction index.

Fig. 5 shows the "hybridization curve" obtained from the application of Eq. (1) to the Bi2 *s*–Bi2 *p* orbitals (accumulated for all *p* orientations). In this case, the evidence coming from the PDOS and the COHP curves is translated into real cation *s*–*p* hybridization, which is seen in all three regions. The mixing of cation *s* and *p* states, which is usually related to distorted coordination environments and stereochemically active lone pairs [5,6], is seen explicitly to originate through their coupling to anion *p*-orbitals. Even though the "secondary interactions" picture is compelling, it is not really necessary to think of the complete interaction as a two-step process. Any coupling in the Hamiltonian which mixes Bi *s* and Bi *p*, even indirectly, can result in wavefunctions with non-zero contributions for both.

The situation is rather different for the Bi1 site. Despite the sizable overlap of the Bi1 *s*–S2 *p* and Bi1 *p*–S2 *p* COHP curves, the *s* and *p* orbitals of the Bi1 atom are not hybridized. The hybridization curve for Bi1 *s*–Bi1 *p* would appear as a horizontal line in Fig. 5 as the values of are several orders of magnitude smaller than those corresponding to the Bi2 site. This could have been predicted qualitatively, since the 2/*m* site symmetry involves a center of inversion and is thus incompatible with any net hybridization that might introduce a polar asymmetry (let alone generate a stereochemically active lone pair).

On the other hand, a difference between the Bi1–S1 and Bi1–S2 behaviors could be expected, since a directional dependence of the electronic configuration is compatible with the specific site symmetry of Bi1 and might be influenced by the different character of the atom groups, in which S1 and S2 participate, in terms of their bonding and structural freedom. Even though the Bi1 octahedron is nearly ideal with six bond lengths of 2.84 Å, S1 is bonded to three Bi atoms, whereas S2 is bonded to three Cu atoms and has only one medium-to-long contact to Bi.

Additional pictorial support for the analysis of the lone-pair expression can be obtained by the consideration of the ELF [22,23]. We provide plots in the Supplementary Material.

Table 2
ICOHP ($\times 10^3$) for the Bi1 and Bi2 sites in $Cu_4Bi_5S_{10}$. The six groups of interactions correspond to the first six lines in Table 1.

Bond	Reg I	Reg IIa	Reg IIb	Reg III
Bi1 *s*–S1 *p*	−9	1	44	5
Bi1 *p*–S1 *p*	0	−49	−2	122
Bi1 *s*–S2 *p*	−14	22	30	3
Bi1 *p*–S2 *p*	0	−35	−13	104
Bi2 *s*–S1 *p*	−17	32	20	38
Bi2 *p*–S1 *p*	0	−73	−10	185
Bi2 *s*–S4 *p*	−18	31	25	25
Bi2 *p*–S4 *p*	0	−56	−16	155
Bi2 *s*–S2 *p*	−5	11	12	−2
Bi2 *p*–S2 *p*	0	−21	−2	58
Bi2 *s*–S3 *p*	−1	1	6	0
Bi2 *p*–S3 *p*	0	−12	0	31

3.2. Charge density of $Cu_4Bi_5S_{10}$

Charge density maps help to visualize the distribution of charge in the crystal structure. Fig. 6a and b shows sections cutting through Bi2 and S1 (the 010-plane), and S4, Bi2 and S2 (∼⊥[100]), respectively. Both cross sections show charge in the energy range of regions I and II. The low charge at the center of the atoms is an effect of the pseudopotentials used in the calculations.

Attention should be drawn to the following features of the Bi2 charge density maps: a strong shared charge can be observed between Bi2 and S1, and Bi2 and S4. The density of charge seen between Bi2 and S2 is clearly weaker. This feature is further pronounced between Bi2 and S3 (not shown in the two cross sections). These observations are in agreement with the bond lengths (Table 1) and ICOHP (Table 2) as the strongest shared charge lies along the shortest bonds and between the atoms showing the largest interactions in the ICOHP. A strong

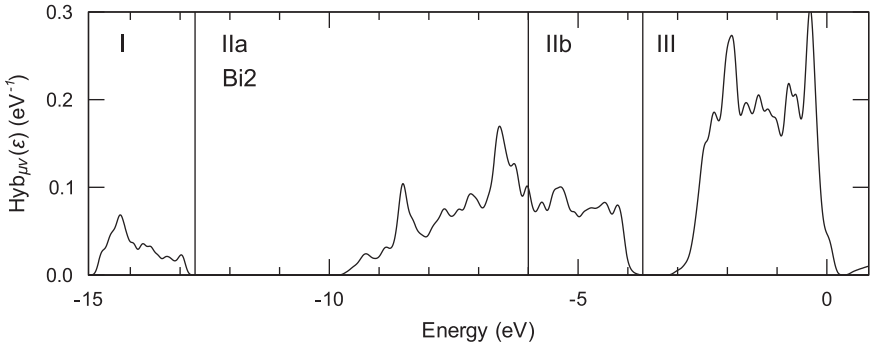

Fig. 5. Hybridization curve for Bi2 *s*–Bi2 *p* in $Cu_4Bi_5S_{10}$. The curve is calculated using Eq. (1).

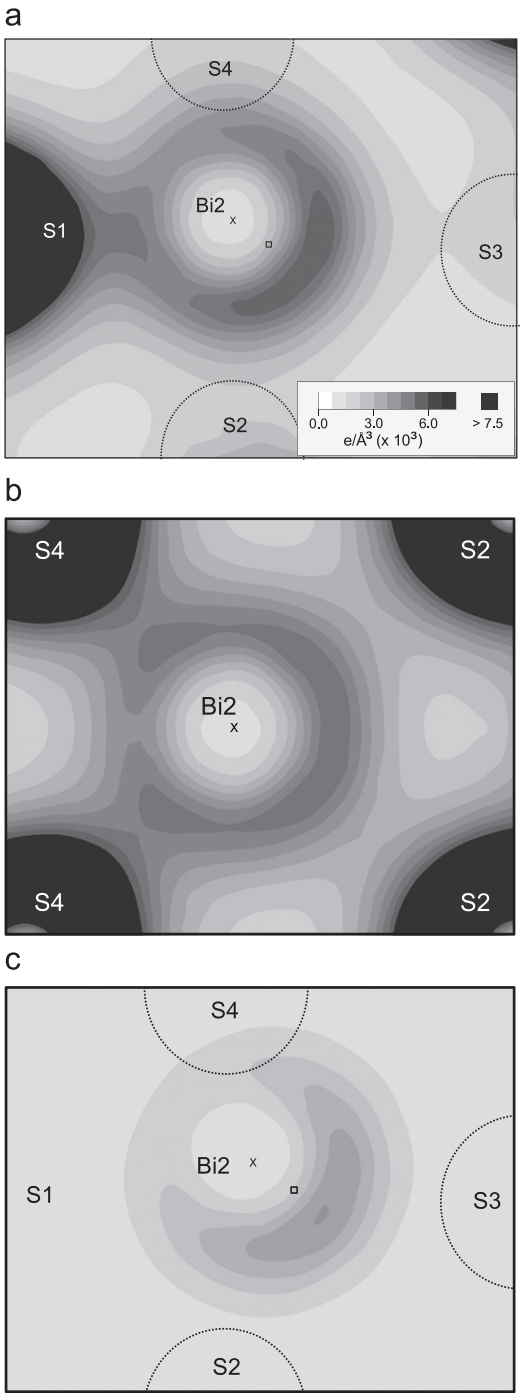

Fig. 6. Partial charge density map sections of $Cu_4Bi_5S_{10}$ through Bi2 parallel to (010) (a) and $\sim\perp$ to [100] (b). (c) shows the same section as (a) but has only the contributions from Bi2 *s* to Bi2 *p*. All maps show density of charge in the energy range of regions I and II. Dashed atoms are above and below the shown planes. A cross indicates the atom position of Bi2 and a square indicates the polyhedron centroid. The scale in (a) applies to all three maps.

concentration of charge is observed on the side of Bi2 facing into the void between two S2 and two S3. This charge can be described as a Bi lone pair which is clearly not shared with the coordinating sulfurs. Removing the contributions from all orbitals except Bi *s* and Bi *p* results in the charge density map shown in Fig. 6c where the lone pair represents the predominant charge. Thus this charge consists of the mixed contributions of Bi *s* and Bi *p*, but the lone pair is, as seen from the PDOS and COHP, eventually an effect of the mixing of both Bi orbitals with S *p*. The distribution of charge in Fig. 6c is in agreement with the model suggested by Walsh and Watson [6], saying that the cation orbitals interfere destructively on one side (towards S1 and S4) and constructively on the opposite side (towards S2 and S3).

The polyhedron centroid is marked along with the atom position of Bi2 in Fig. 6a and c. The Bi2 atom is displaced from the centroid in a direction opposite to the lone pair. This confirms the crystal chemical interpretation of the orientation of the lone pair.

Charge density maps for the Bi1 polyhedron in the full energy range of regions I and II show a predominantly spherical distribution of charge around Bi1 with shared charge between Bi1 and each of the six coordinating sulfurs (not illustrated). The energy range in Fig. 7 is narrowed down to region IIb in order to investigate the specific features in the region where Bi1–S1 has pure anti-bonding character and Bi1–S2 shows overlap between COHP curves. Fig. 7a shows the density of charge in a section which includes Bi1 and the four coordinating S1 atoms. The Bi1 *s*–S1 *p* anti-bonding interaction results in a weak charge around Bi1 with no specific concentrations in this plane. The distribution

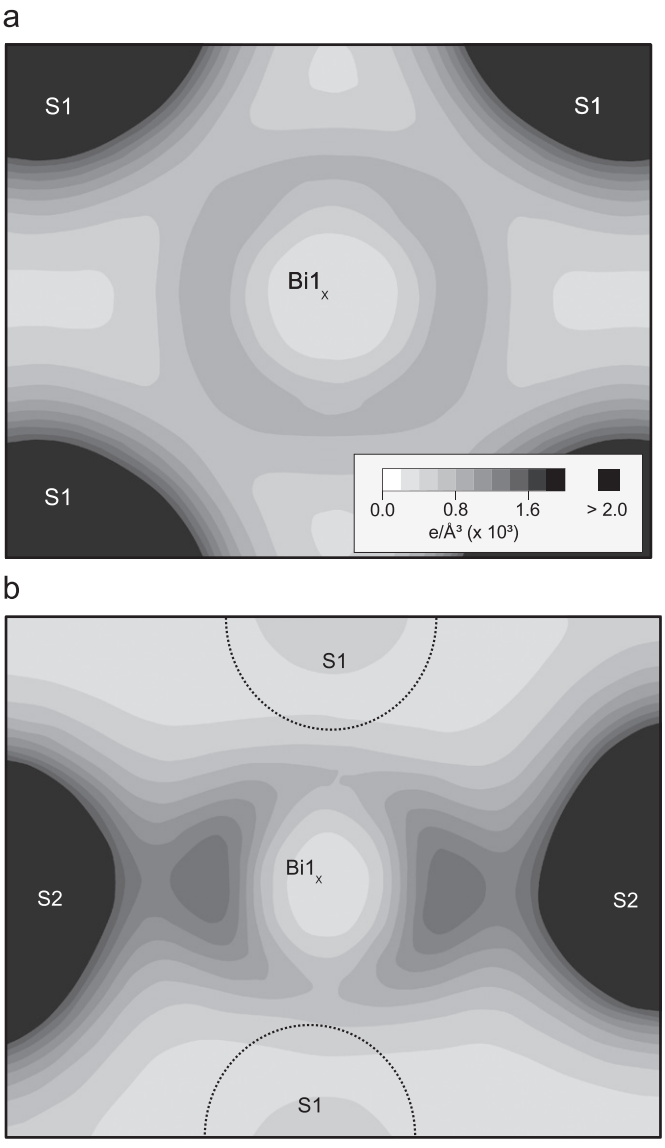

Fig. 7. Partial charge density map sections of $Cu_4Bi_5S_{10}$ through Bi1 with the orientations $\sim\perp$ [100] (a) and parallel to (010) (b). The maps show density of charge in the energy range of region IIb. Dashed atoms are above and below the shown planes. A cross indicates the atom position of Bi1. The scale in (a) also applies to (b).

of charge looks different in a section oriented to include Bi1 and the two coordinating S2 atoms (Fig. 7b). A double-lobed charge is concentrated on Bi1 pointing towards S2. The above discussion of the electronic structure suggests that this is not an effect of any Bi *s*–Bi *p* hybridization in this direction, but simply a superposition of the charge densities associated to the *s* and *p* orbitals separately. In contrast to the case of Bi2, this "diagonal" superposition does not introduce any asymmetry.

3.3. Conclusions on $Cu_4Bi_5S_{10}$

The study on $Cu_4Bi_5S_{10}$ has shown indications of Bi *s*–Bi *p* hybridization at the Bi2 site resulting from the Bi *s*–S *p* and Bi *p*–S *p* interactions. The mixing of orbitals on this site occurs in a distorted coordination environment and shows charge density features interpreted as a lone pair. The distribution of charge is in line with observations from other lone pair studies [5,6]. The lone pair is oriented towards the longest Bi–S distances in the polyhedron but does not extend far from the bismuth atom.

The Bi1 site is a symmetrical environment and no indications of Bi *s*–Bi *p* hybridization are found, despite the existence of sizable Bi *s*–S *p* and Bi *p*–S *p* interactions and some degree of overlap between the respective COHP curves. It is clear that the site symmetry (a minimal 2/*m*, but with a crucial center of inversion) is responsible for the absence of *s*–*p* mixing.

4. Bi_2S_3

The crystal structure of Bi_2S_3 has been studied in detail between 0 and 9.2 GPa in a single crystal X-ray diffraction experiment [12]. Starting from the experimental data we have performed a full optimization of the lattice parameters and atomic positions at several pressures within the experimental pressure range. The calculated equilibrium volume of Bi_2S_3 at zero pressure is 515.1 Å^3 in fair agreement with the experimental value of 498.4(7) Å^3. Table 3 compares the Bi–S interatomic distances of the *ab initio* and experimental structures at 0 and 9.2 GPa.

The crystal structure of Bi_2S_3 has two distinct cation sites both coordinated by seven sulfurs (Fig. 8). Looking along the *b*-axis the Bi1 polyhedron is a lying-down mono-capped trigonal prism, whereas the Bi2 polyhedron is a standing mono-capped trigonal prism. There are small differences in the distribution of bond lengths for the two sites at room pressure (Table 3). Bi1 exhibits three short-to-intermediate bonds plus four substantially longer ones, similar to Bi2 and Bi3 in $Cu_4Bi_5S_{10}$, whereas Bi2 has one short bond, four intermediate and two long bonds. No phase transition is observed in Bi_2S_3 within the studied pressure range and the bond lengths show a continuous evolution with pressure. At room pressure Bi1 and Bi2 have cation eccentricities of 0.142 and 0.160 (values from the *ab initio* calculations), respectively, decreasing to 0.043 and 0.087 at 9 GPa. Both sites get less asymmetric with pressure, but some cation eccentricity is still present and they never reach a fully isotropic geometry within this pressure range.

Table 3
Comparison of bond lengths (Å) in the *ab initio* and experimental [12] Bi_2S_3 crystal structures at 0 GPa/**9** GPa.

Bond	*Ab initio*	Experimental
Bi1–S2 (× 2)	2.71/**2.71**	2.64/**2.67**
Bi1–S3	2.73/**2.78**	2.69/**2.74**
Bi1–S2	3.01/**2.79**	3.05/**2.78**
Bi1–S1 (× 2)	3.06/**2.87**	3.03/**2.85**
Bi1–S3	3.47/**2.91**	3.39/**2.91**
Bi2–S1	2.63/**2.67**	2.59/**2.63**
Bi2–S3 (× 2)	2.76/**2.72**	2.74/**2.68**
Bi2–S1 (× 2)	2.98/**2.89**	2.98/**2.87**
Bi2–S2 (× 2)	3.36/**3.03**	3.33/**3.01**

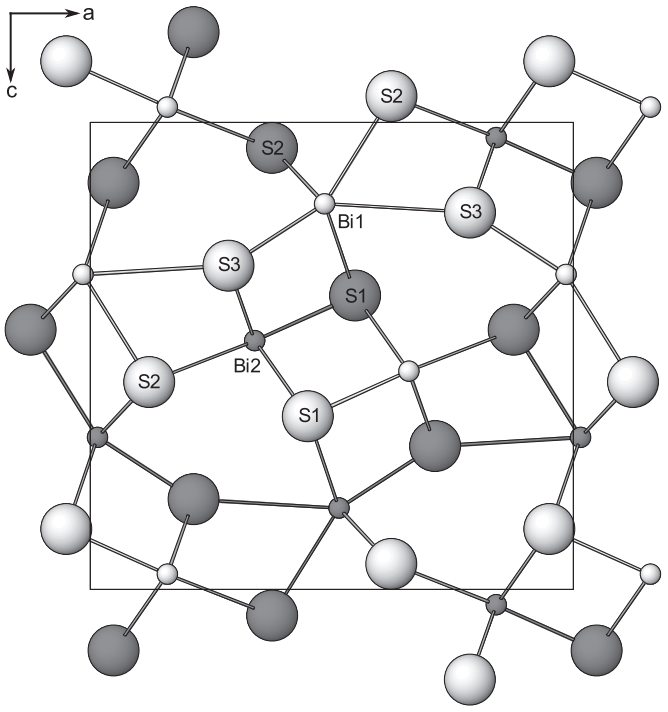

Fig. 8. Crystal structure of Bi_2S_3 at 0 GPa. Dark circles represent atoms on the $y=0.25$ mirror plane, white circles represent atoms on the $y=0.75$ mirror plane.

4.1. Electronic structure of Bi_2S_3

In the following section the focus will be on the Bi1 polyhedron, which is the one showing the largest change as a function of pressure. The calculations for Bi2 are presented in Supplementary Material. The study will be limited to the pressure range of the experimental data where we know that the crystal structure is stable. Fig. 9 shows the PDOS for Bi1 and S1. The main features of the PDOS of Bi_2S_3 at 0 GPa are similar to what has been described for both types of sites in $Cu_4Bi_5S_{10}$. Region I contains a band which has contributions from Bi *s* and S *p* and is split off from the upper valence band. The upper valence band in region II spans from approximately −9 eV to the Fermi level at −4.5 eV. This band has contributions from all orbitals. Region II is subdivided in regions IIa and IIb based on a pronounced change in the number of Bi *s*, Bi *p* and S *p* states between the two subregions. Region III is the lowest part of the conduction band and contains mainly Bi *p* and S *p* states. The Bi *s* states in region IIb are concentrated in a peak close to the Fermi level. This is in contrast to the situation in $Cu_4Bi_5S_{10}$ where the Bi *s* states have a broader distribution. The increment of pressure from 0 to 9 GPa does not substantially change the PDOS of Bi_2S_3 (Fig. 9). The PDOS flattens and the band gaps are closing, with a simultaneous slight decrease in the number of Bi *p* states in region IIb.

The COHP averaged over the three shortest bonds in the Bi1 polyhedron is shown in Fig. 10. Looking at the COHP at 0 GPa we again see the same main features as described for $Cu_4Bi_5S_{10}$. The bonding part of the Bi *s*–S *p* interactions is found in the energy range of region I and the anti-bonding part is distributed in region II with the main contribution in region IIb. Bi *p*–S *p* is bonding in region II and anti-bonding in region III. By comparing the details of the COHP of Bi1 in Bi_2S_3 at 0 GPa with the asymmetric Bi2 site in $Cu_4Bi_5S_{10}$ (Fig. 4) we observe differences in the distribution of interactions in region II. The Bi2 site in $Cu_4Bi_5S_{10}$ has a strong

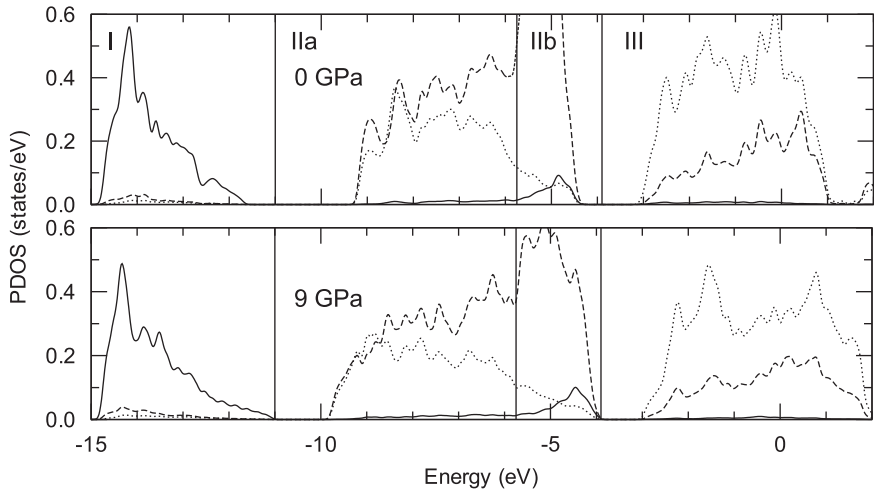

Fig. 9. PDOS for Bi1 and S1 in Bi_2S_3 at 0 and 9 GPa. Dashed line is S *p*, solid line is Bi *s* and dotted line is Bi *p*.

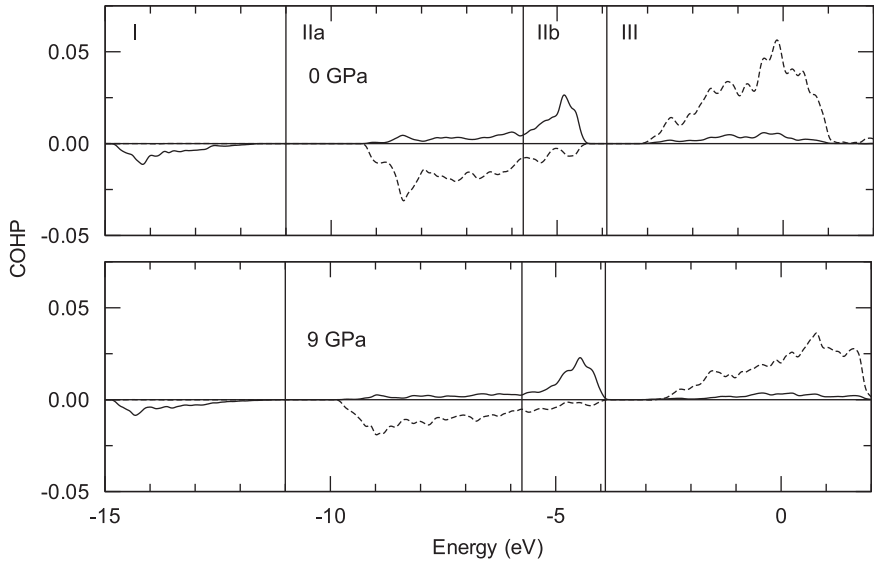

Fig. 10. COHP per bond for the Bi1–S (only the three shortest bonds are taken into account) interactions in Bi_2S_3. Solid lines are used for Bi *s*–S *p* interactions, dashed for Bi *p*–S *p*. A negative COHP value means a bonding interaction.

Bi *s*–S *p* interaction at the top of region IIa, whereas the corresponding interaction for Bi1 in Bi_2S_3 is more concentrated in region IIb, closer to the Fermi level. Although both sites are asymmetric, they have different coordination environments which are reflected in the COHP. However, a common feature of the COHPs is the presence of Bi *s*–S *p* interactions in region IIa and Bi *p*–S *p* in region IIb. For the Bi1 site in Bi_2S_3, the curves, resulting from the application of Eq. (1), shown in Fig. 11 confirm that there is a corresponding Bi *s*–Bi *p* hybridization.

The quantification of interactions in Table 4 shows a simple relationship between ICOHP and bond length in Bi_2S_3 at 0 GPa. The ICOHP is very similar for the three shortest bonds (one Bi1–S3 and two Bi1–S2) and they comprise the main interactions in the polyhedron. The interactions along the four longer bonds are markedly weaker and the Bi *s*–S *p* and Bi *p*–S *p* are more concentrated in region IIb and region IIa, respectively.

The COHP of the three short bonds decreases as the pressure is increased from 0 to 9 GPa. This can be seen in both Fig. 10 and Table 4. The ICOHP of the short Bi1–S2 bond decreases in most regions despite an unchanged bond length of 2.71 Å. The length of the Bi1–S3 bond increases from 2.73 to 2.78 Å and this is reflected in an overall decrease in ICOHP. The decrease in ICOHP along the three shortest distances is a general effect of the rearrangement of bonding interactions as the ICOHP of the four longer bonds increases at higher pressure. This is in agreement with the marked shortening of the latter four bonds.

The curves of Bi *s*–Bi *p* hybridization on Fig. 11 suggest that the degree of *s*–*p* mixing is only slightly reduced in going from 0 to 9 GPa, following the aggregate trend of the ICOHP, and becomes somewhat more extended in energy.

4.2. Charge density of Bi_2S_3

In the experimental study on Bi_2S_3 by Lundegaard et al. [12] the orientation of the Bi1 lone pair was estimated from the atom position and the polyhedron centroid. Based on this geometrical approach the lone pair at 0 GPa is facing the S3 atom which is 3.47 Å away from Bi1. The charge density map in Fig. 12a shows a section of the 010-plane which cuts through Bi1 and three of the coordinating sulfurs. The distribution of charge clearly supports the geometrical interpretations [12]. The cation is shifted away from

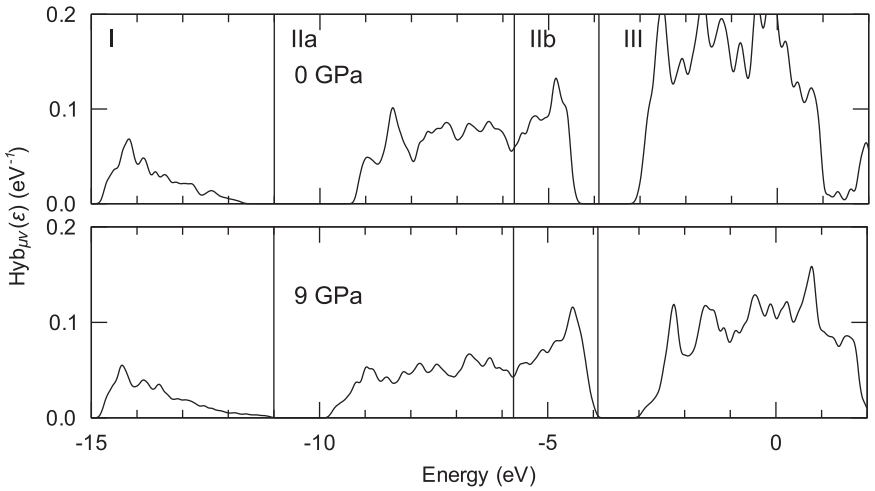

Fig. 11. Hybridization curves for Bi1 *s*–Bi1 *p* in Bi_2S_3 at 0 and 9 GPa. The curves are calculated using Eq. (1).

Table 4
ICOHP ($\times 10^3$) at 0/**9** GPa for the Bi1 site in Bi_2S_3. The rows are ordered according to increasing interatomic distances. The five groups of interactions correspond to the first five lines in Table 3.

Bond	Reg I	Reg IIa	Reg IIb	Reg III
Bi1 *s*–S2 *p*	−13/−**12**	10/**8**	19/**22**	12/**10**
Bi1 *p*–S2 *p*	0/**0**	−61/−**47**	−7/−**8**	112/**91**
Bi1 *s*–S3 *p*	−11/−**8**	10/**6**	17/**17**	11/**7**
Bi1 *p*–S3 *p*	0/**0**	−53/−**38**	−9/−**5**	105/**74**
Bi1 *s*–S2 *p*	−4/−**8**	0/**3**	16/**24**	−1/**1**
Bi1 *p*–S2 *p*	0/**0**	−29/−**39**	−1/−**7**	55/**78**
Bi1 *s*–S1 *p*	−3/−**7**	1/**4**	12/**18**	2/**4**
Bi1 *p*–S1 *p*	0/**0**	−26/−**35**	2/**1**	47/**61**
Bi1 *s*–S3 *p*	−1/−**5**	0/**4**	3/**15**	0/**3**
Bi1 *p*–S3 *p*	0/−**1**	−10/−**30**	2/**2**	12/**48**

the polyhedron centroid and the strongest charge on Bi1 is concentrated in a direction opposite to the shift. This charge can be interpreted as a lone pair as it is concentrated on the bismuth atom and not shared with S3. A strong shared charge can be seen along the short Bi1–S3 (Fig. 12a) and Bi1–S2 (Fig. 12b) bonds. The density of charge is weaker between Bi1–S1 and the longer Bi1–S2, in accordance with the ICOHP and the bond lengths (Tables 3 and 4).

The effect of increased pressure is evident in the charge density maps (Fig. 13). The charge around Bi1 becomes more evenly distributed and the characteristic shape of the lone pair is greatly reduced. The atom position and polyhedron centroid are very close at 9 GPa and this leaves a very limited space for a lone pair. The interatomic distance between Bi1 and S3 which is 3.47 Å at 0 GPa is decreased to 2.91 Å at 9 GPa and a stronger shared charge can now be observed between the two atoms. The weak shared charge between Bi1–S1 and the longer Bi1–S2 at 0 GPa is enhanced as the bonds are markedly shortened. The weakening of interactions along the three short bonds in the ICOHP is not clearly seen in the charge maps.

ELF plots which support the analysis for the Bi1 site in Bi_2S_3 at 0 and 9 GPa are provided in the Supplementary Material.

4.3. Conclusions on Bi_2S_3

The theoretical calculations show, in accordance with the experimental study, that the coordination environment of the Bi1 site in Bi_2S_3 changes with pressure. The variation in bond lengths is equalized at higher pressure and this is reflected in the ICOHP. The interactions are decreased along the three short bonds and increased along the four longer bonds. The degree of Bi *s*–Bi *p* hybridization decreases slightly, and the distinct shape of the lone pair which is seen in the charge density map at 0 GPa is reduced with increasing pressure. Although the Bi1 site in Bi_2S_3 becomes more regular with pressure no restrictive site symmetry in addition to the (010) mirror plane is applied and the coordinating sulfurs are assumed to have a more uniform bonding character. Hence, despite the existence of a certain degree of Bi *s*–*p* mixing, the reduction of the anisotropy brought about by pressure hampers the expression of an stereochemically active lone pair.

5. General conclusions

The crystal structure of $Cu_4Bi_5S_{10}$ is interesting as it has both symmetric and asymmetric coordination environments for bismuth. The detailed study of the asymmetric site confirms a number of observations from related studies. In particular, the analysis is compatible with the view that Bi *s*, Bi *p* and S *p* are all mixed in the same wavefunctions, with the two former orbitals forming a local cation hybrid. A charge density map of the asymmetric site shows a lone pair which is oriented along the longest interatomic distances in the coordination polyhedron. The Bi at the symmetric site exhibits coupling to the S *p* neighbor orbitals and some degree of overlap between the Bi *s*–S *p* and Bi *p*–S *p* COHP curves, but this does not result in an effective *s*–*p* mixing of the Bi orbitals.

The effect of pressure on Bi–S interactions has been studied in Bi_2S_3. The coordination environment of Bi is asymmetric at 0 GPa and the electronic characteristics resemble those of the asymmetric sites in $Cu_4Bi_5S_{10}$. The shortest bonds contribute most to the effective interactions leading to Bi *s*–Bi *p* hybridization and a lone pair is clearly seen in the charge density maps. The variation in bond lengths is equalized as pressure is increased from 0 to 9 GPa and the characteristic shape of the lone pair is greatly reduced in the charge density map, in a manner that suggests that the only slightly reduced *s*–*p* hybridization at 9 GPa seems to be expressed more evenly around Bi.

The lone pair at distorted sites is oriented in a direction opposite to the displacement of the cation from the polyhedron centroid. This confirms that the displacement can be used to determine the orientation of the lone pair for distorted sites. The

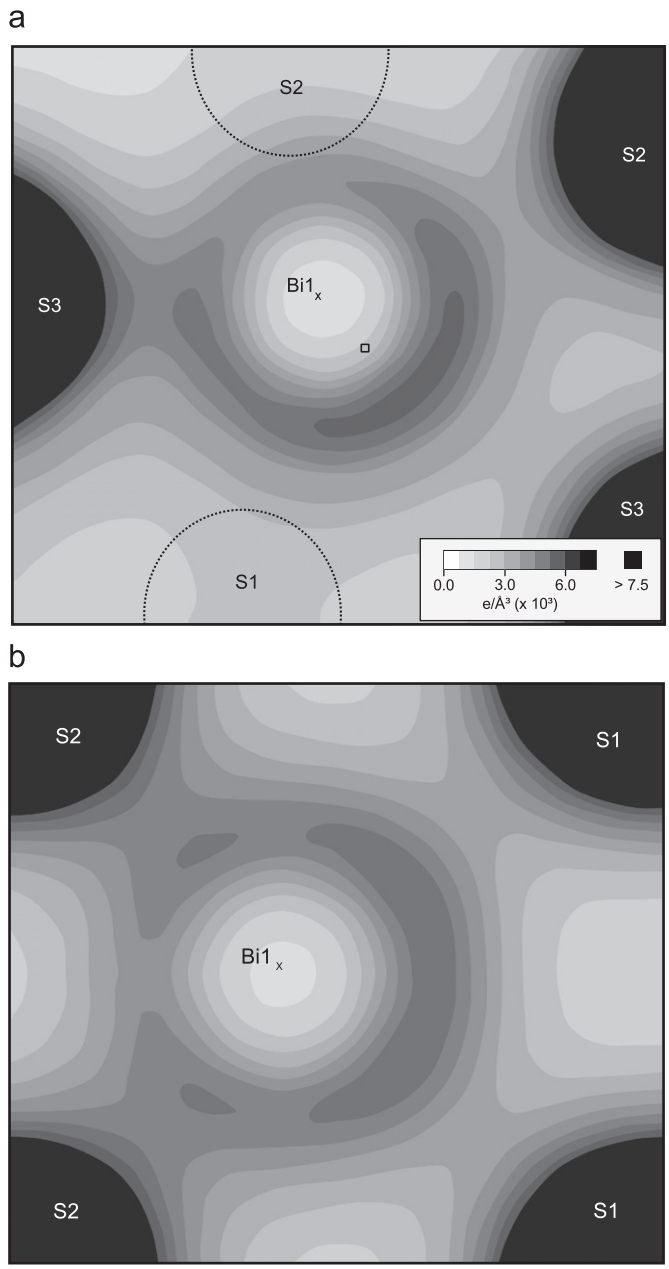

Fig. 12. Partial charge density map sections of Bi_2S_3 through Bi1 parallel to (010) (a) and ~ parallel to (−101) (b). The maps show density of charge in the energy range of regions I and II at 0 GPa. Dashed atoms are above and below the shown planes. A cross indicates the atom position of Bi1 and a square indicates the polyhedron centroid. The scale in (a) also applies to (b).

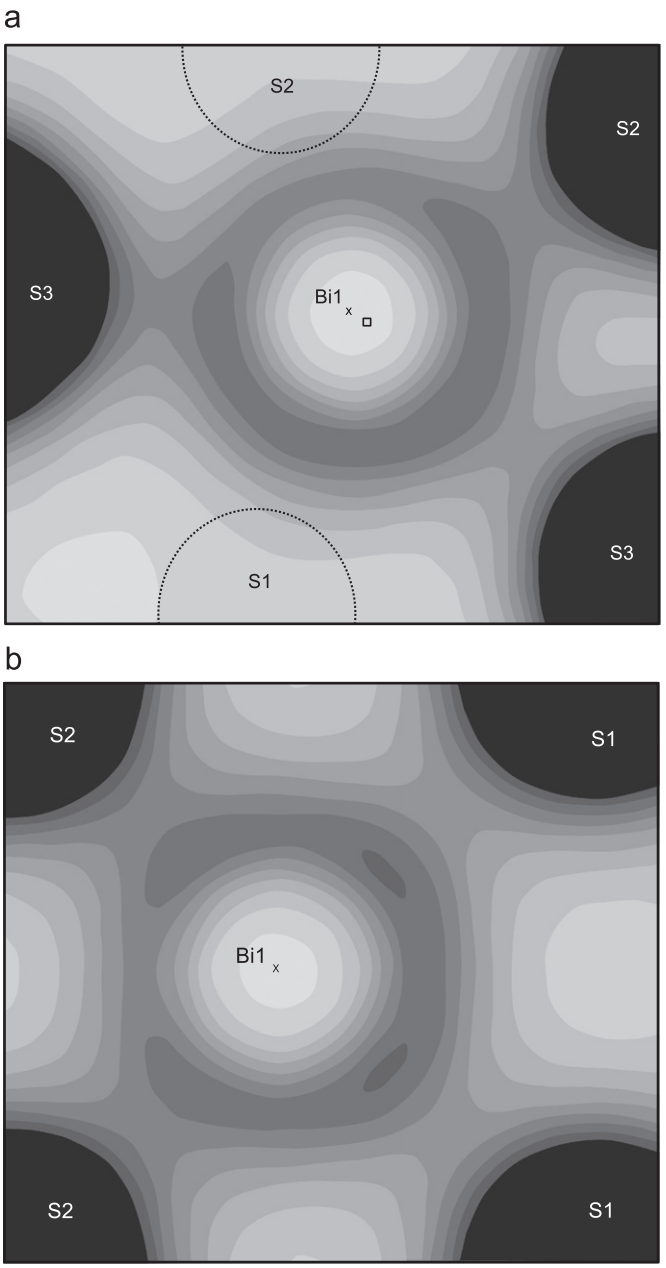

Fig. 13. Partial charge density map sections of Bi_2S_3 parallel to (010) (a) and ~ parallel to (−101) (b). The maps show density of charge in the energy range of regions I and II at 9 GPa. Dashed atoms are above and below the shown planes. A cross indicates the atom position of Bi1 and a square indicates the polyhedron centroid. The same scale as in Fig. 13 is used.

cation approaches the centroid as the pressure is increased and the characteristic shape of the lone pair is reduced in the charge density maps. The cation eccentricity is thus correlated to the degree which the lone pair appears as a lobe of non-shared charge.

We have seen that despite the existence of a certain degree of Bi *s*–*p* mixing, the reduction of the anisotropy brought about by pressure hampers the expression of a lone pair. The lone pair itself has an influence in the elastic properties of the system (i.e., in its response to the external pressure). In the event, the geometrical distortion and the existence of a lone pair are both consequences of the ultimate ground state of the system, and it is not really appropriate to focus on which feature comes first and which is caused by the other.

As a final thought: this kind of electronic-structure analysis describes the state of affairs for a given structure, but is unable to predict whether a given system will exhibit a structural instability leading to a low-symmetry coordination polyhedron and the appearance of a lone-pair. That will be determined in general by effects outside the scope of this discussion.

Acknowledgments

This work was supported by the European Science Foundation (ESF) under the EUROCORES Programme EuroMinSci (www.esf.org/eurominsci), through Contract no. ERAS-CT-2003-980409 of the European Commission, DG Research, FP6, and by the national funding

agencies of Spain (Grants CGL2005-2095-E, FIS2006-12117-C04-01, FIS2008-03834, FIS-2009-12721-C04-03 and CSD2007-00045) and Denmark (Grants 272-08-0233 and 272-08-0227).

Appendix A. Supplementary Material

Supplementary data associated with this article can be found in the online version at doi:10.1016/j.jssc.2010.07.022.

References

[1] L.E. Orgel, J. Chem. Soc. (1959) 3815.
[2] H.J. Terpstra, R.A. de Grott, C. Haas, Phys. Rev. B 52 (1995) 11690.
[3] G.W. Watson, S.C. Parker, G. Kresse, Phys. Rev. B 59 (1999) 8481.
[4] G.W. Watson, J. Chem. Phys. 114 (2001) 758.
[5] A. Walsh, G.W. Watson, J. Solid State Chem. 178 (2005) 1422.
[6] A. Walsh, G.W. Watson, J. Phys. Chem. B 109 (2005) 18868.
[7] J. Yang, M. Dolg, Phys. Chem. Chem. Phys. 9 (2007) 2094.
[8] J. Raulot, G. Baldinozzi, R. Seshadri, P. Cortona, Solid State Sci. 4 (2002) 467.
[9] M.W. Stoltzfus, P.M. Woodward, R. Seshadri, J. Klepeis, B. Bursten, Inorg. Chem. 46 (2007) 3839.
[10] A. Mudring, Eur. J. Inorg. Chem. (2007) 882.
[11] L.F. Lundegaard, R. Miletich, T. Balić-Žunić, E. Makovicky, Phys. Chem. Minerals 30 (2003) 463.
[12] L.F. Lundegaard, E. Makovicky, T. Boffa-Ballaran, T. Balić-Žunić, Phys. Chem. Minerals 32 (2005) 578.
[13] L.A. Olsen, T. Balić-Žunić, E. Makovicky, A. Ullrich, R. Miletich, Phys. Chem. Minerals 34 (2007) 467.
[14] L.A. Olsen, T. Balić-Žunić, E. Makovicky, Inorg. Chem. 47 (2008) 6756.
[15] T. Balić-Žunić, E. Makovicky, Acta Cryst. B52 (1996) 78–81.
[16] J.M. Soler, E. Artacho, J.D. Gale, A. García, J. Junquera, P. Ordejón, D. Sánchez-Portal, J. Phys. Condens. Matter 14 (2002) 2745.
[17] R. Dronskowski, P.E. Blöchl, J. Phys. Chem. 37 (1993) 8617.
[18] J.P. Perdew, K. Burke, M. Ernzerhof, Phys. Rev. Lett. 77 (1996) 3865.
[19] E. Anglada, J.M. Soler, J. Junquera, E. Artacho, Phys. Rev. B 66 (2002) 205101.
[20] K. Mariolacos, V. Kupčík, M. Ohmasa, G. Miehe, Acta Cryst. B31 (1975) 703.
[21] D. Topa, E. Makovicky, T. Balić-Žunić, W.H. Paar, Can. Mineral. 41 (2003) 1155.
[22] A.D. Becke, K.E. Edgecombe, J. Chem. Phys. 92 (1990) 5397.
[23] A. Savin, O. Jepsen, J. Flad, O.K. Andersen, H. Preuss, H.G. von Schnering, Angew. Chem. Int. Ed. Engl. 31 (1992) 187.